PHYSICAL REVIEW B VOLUME 51, NUMBER 8 15 FEBRUARY 1995-II

Growth kinetics of CaF_2/Si(111) heteroepitaxy: An x-ray photoelectron diffraction study

J. D. Denlinger* and Eli Rotenberg*
Department of Physics and Lawrence Berkeley Laboratory, University of California, Berkeley, California 94720

U. Hessinger, M. Leskovar, and Marjorie A. Olmstead
Department of Physics, FM-15, University of Washington, Seattle, Washington 98195
(Received 6 June 1994)

Kinetic variations of the initial stages of CaF_2 growth on Si(111) by molecular-beam epitaxy are studied with the *in situ* combination of x-ray photoelectron spectroscopy and diffraction. After the formation of a chemically reacted interface layer, the morphology of the subsequent bulk layers is found to be dependent on the substrate temperature and incident flux rate, as well as the initial interface structure. For substrate temperatures above $\sim 600\,^{\circ}\mathrm{C}$, subsequent layers do not easily wet the interface layer, and a transition is observed from a three-dimensional island formation at low flux to a laminar growth following the coalescence of bilayer islands at higher flux. At lower substrate temperatures ($\sim 450\,^{\circ}\mathrm{C}$), a different stoichiometry and structure of the interface layer leads to laminar growth at all fluxes, but with a different bulk nucleation behavior. Crystalline heteroepitaxy is not observed when growth initiates at room temperature, but homoepitaxy does proceed at room temperature if the first few layers are deposited at a high temperature. The different growth regimes are discussed in terms of a kinetic model separating step and terrace nucleation where, contrary to homoepitaxy, step nucleation leads to islanded growth.

I. INTRODUCTION

In heteroepitaxial growth, the relative surface energies of the overlayer and substrate are commonly used to predict equilibrium laminar or islanding growth behavior. Despite the inherent nonequilibrium nature of molecular-beam epitaxy (MBE), these thermodynamic energy arguments, augmented by strain-energy considerations for lattice-mismatched systems, are powerful predictors of growth morphology when the two materials are chemically similar. However, the nonequilibrium rates of surface diffusion, nucleation, and interlayer transport, i.e., growth kinetics, also play an important role in determining initial growth morphologies. Even in homoepitaxy, kinetic constraints may lead to departures from equilibrium surface structures during growth.[1,2]

In the case of heteroepitaxial growth of dissimilar materials, interface reactions can alter both the relevant surface energies and the kinetic parameters during the initial stages of epitaxy. For the system of CaF_2 on Si(111), an ionic insulator nearly lattice matched to a covalent semiconductor, a strong chemical reaction at the interface results in the formation of a nonwetting surface and an islanded pathway to subsequent CaF_2 homoepitaxy that depends on kinetics.[3–5] The key experimental kinetic parameters are the incident flux (surface adatom concentration), substrate temperature (diffusion and transport barriers), and surface orientation (terrace widths and step structure). In this paper, we explore the flux and temperature regimes that govern the formation of this chemisorbed interface layer and the nucleation of subsequent bulk layers, and discuss the underlying kinetics and energetics.

Thin [0.5–8 triple layer (TL)] CaF_2-on-Si(111) films were grown using MBE and characterized *in situ* using a combination of x-ray photoelectron spectroscopy (XPS) and component-resolved x-ray photoelectron diffraction (CR-XPD), which allows simultaneous determination of both their atomic structure and overall morphology. We identify several distinct growth regimes: For temperatures above about $600\,^{\circ}\mathrm{C}$, we find a complete, reacted Si-Ca-F layer. At high fluxes, subsequent growth on this layer proceeds as 2-layer-high islands that coalesce, followed by layer-by-layer growth; at lower fluxes, we find the reacted Si-Ca-F layer to be partially covered with thick islands. At lower temperatures ($\sim 450\,^{\circ}\mathrm{C}$), the interface becomes an incompletely occupied Si-Ca-F_x ($x \sim 2$) layer, which does not fully cover the substrate before nucleation of subsequent layers; once covered, however, the growth proceeds approximately layer-by-layer. At room temperature, the incomplete interface reaction leads to amorphous or polycrystalline films, although highly crystalline films may be grown at room temperature if the first few layers are grown at high temperatures. In all cases except the amorphous growth, we find the buried interface structure to be identical to the unburied Si-Ca-F layer, overlaid with bulk-structure CaF_2.

With XPS, photoelectron kinetic-energy distributions map the electronic structure of the substrate and overlayer and provide elemental- and chemical-state identification. With XPD, we measure and interpret the angular distribution of photoelectron intensities. Forward-scattering enhancements of the photoelectron signal along interatomic axes at moderately high-electron kinetic energies (>200 eV), provide structural information about crystalline materials.[6–8] In addition, binding

0163-1829/95/51(8)/5352(14)/$06.00 ©1995 The American Physical Society

energy shifts in XPS allow component-resolved XPD to discriminate the local structure of different chemical species. In this paper, we make use of the well-known Ca-Si interface binding-energy signature[9–12] to separate bulk and interface Ca $2p$ XPD. Elsewhere,[13] we have exploited forward-scattering enhancements to identify the small energy splittings between surface and bulk emission, and between buried and unburied interface emission for both Ca and F. In the present work, however, we will quantify growth morphology treating the bulk and surface species as one energy component, and buried and unburied interface species as a second component.

We first present the experimental CaF_2 growth conditions, demonstrate XPD data collection for a clean substrate and a thick overlayer film, and discuss the XPD structural signatures used in our characterization of thin films. In Sec. III, different initial nucleation behaviors at high and low substrate temperatures are demonstrated with single-component-interface XPD. Bulk and interface Ca $2p$ CR-XPD is then used in Sec. IV to identify and characterize the distinct growth regimes as a function of temperature and flux; a nonisothermal template growth technique is also briefly discussed. In Sec. V, a complementary picture of the growth morphologies is given based on F $1s$ and *KVV* XPD. Finally, we delineate the kinetic regimes with an isothermal-growth phase diagram and discuss kinetic origins of the growth modes.

II. EXPERIMENT

A. Growth conditions

CaF_2 was evaporated from a Knudsen effusion cell onto resistively heated Si(111) substrates in an ultrahigh vacuum chamber (base pressure $<2\times10^{-10}$ Torr) equipped for XPS/XPD and low-energy electron-diffraction (LEED) analysis. Substrates consisting of 5×15 mm^2 sections of a Si wafer [p-type, 1 Ω cm, $<0.25°$ oriented from (111)] were prepared with a standard wet chemical etch[14] before introduction to the vacuum chamber. After *in vacuo* outgassing of the sample and molybdenum holder to ~600 °C, the protective oxide coating was then desorbed by annealing to ~850 °C until a sharp room-temperature 7×7 LEED pattern was obtained, and no oxygen and $<1\%$ carbon was detectable by XPS. Grazing-incidence 500-eV Ar^+ sputtering was used to remove thin overlayers in order to reuse substrates. The substrate temperature was monitored with an optical pyrometer; observation of LEED simultaneous with annealing indicated a $7\times7\leftrightarrow1\times1$ transition at ~835 °C for clean Si substrates.[15]

Deposition rates were calibrated with a quartz oscillator mass balance. CaF_2 was sublimated from either graphite or pyrolitic-BN (PBN) crucibles. In both cases, heater element contact with BN insulators resulted in N_2 outgassing to $\sim10^{-9}$ (10^{-8}) Torr at a growth rate of ~5 Å/min (~50 Å/min). However, despite this N_2 background pressure during the growth of all films in this study, no nitrogen (or boron) incorporation into the film was evident with XPS. Also, despite early reports of boron contamination-induced cracking of *thick* films grown from PBN crucibles,[16,17] no differences in the *initial* stages of overlayer nucleation studied here were found when the crucible type was changed from PBN to graphite. A mask during growth prevented deposition onto the sample holder. The O $1s$ core level was periodically monitored during the course of an experiment to assess the x-ray irradiation damage to the sample. Due to the sensitivity of CaF_2 to electron-beam exposure,[18] LEED was not performed until after all photoemission data were acquired.

B. XPD data collection

XPS and XPD were performed with Mg K_α x-ray illumination ($h\nu=1253.6$ eV) and photoelectron detection by a 126-mm hemispherical electron-energy analyzer (Leybold EA-11) with a fixed 55° angle between the source and detector. XPS binding energies are reported relative to the Fermi level, calibrated to the Au $4f_{7/2}$ binding energy of -84.0 eV. To acquire XPD data, voltages were altered on the spectrometer input lens to decrease the full-width angular acceptance from $>10°$ to $<4°$, and the energy resolution was relaxed to increase counting statistics. XPD scans were obtained by polar (θ) and azimuthal (ϕ) rotations of the sample, with $\theta=0°$ defining normal emission. To illustrate our XPD data collection and the bulk structures of the substrate and overlayer, we show in Fig. 1 a planar representation of the angle-resolved Ca $2p$ electron emission in the 2π solid angle above the surface of an 8-TL CaF_2 film deposited on Si(111). Data were acquired over the 60° azimuthal sector bounded by the white lines and then symmetrized

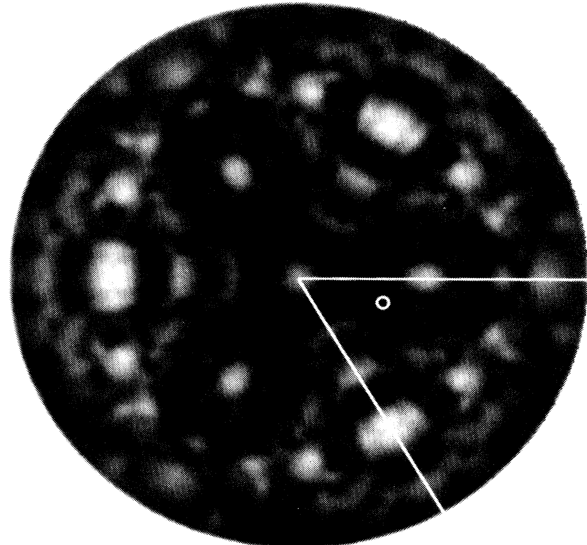

FIG. 1. Ca $2p$ XPD pattern for an 8-TL CaF_2 film on Si(111). Data was collected in the 60° sector shown and then symmetrized to obtain the full 2π planar projection. The white circle indicates an off-axis emission direction used for the intensity analysis without direct forward-scattering enhancements. The CaF_2 film was deposited with a 50-Å/min incident flux at 650 °C substrate temperature.

according to the substrate's C_{3v} symmetry (verified over a limited range of polar scans). This procedure is not completely equivalent to acquiring data over the complete 2π solid angle since the asymmetric orientation of the x-ray source polarization relative to the sample removes the C_{3v} symmetry of the photoemission pattern.

For most samples in this study, conclusions were drawn from two polar scans along the $[11\bar{2}]$ and $[\bar{1}2\bar{1}]$ high-symmetry azimuths at $\phi=0°$ and $\phi=-60°$. These two polar-angle data sets are combined to represent emission in the $(1\bar{1}0)$ plane of the substrate and are presented as negative and positive polar angles relative to the sample normal. Figure 2 shows such polar profiles for Ca 2*p* and F 1*s* emission from an 8-TL film and also Si 2*p* emission from a clean 7×7 Si(111) substrate. Because the areal acceptance of the detector is matched to the width of the sample (at $\theta=0°$), the sample area seen by the detector is constant as a function of polar angle. Hence the nondiffractive angular instrument response is governed primarily by the effective depth of detection D of the outgoing photoelectrons:

$$D \approx \lambda \cos\theta (1 - e^{-t/\lambda\cos\theta}) , \tag{1}$$

where λ is the bulk inelastic attenuation length. This results in $\sim\cos\theta$ profiles for thick film and substrate signals as in Fig. 2(c), and in flat polar profiles for monolayer signals (Sec. III). This slowly varying, noncrystalline background function is normalized to unity at $\theta=0°$ in all XPD polar profiles and was subtracted from the XPD pattern of Fig. 1 for clarity. An off-axis emission direction identified by the white circle in Fig. 1 ($\theta=26°$, $\phi=-18°$) was used for measurement of photoemission intensities minimally influenced by forward scattering and diffraction enhancements.

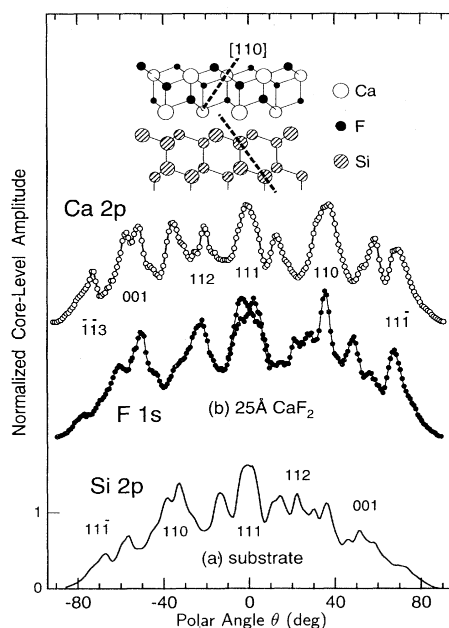

FIG. 2. Core-level XPD polar profiles for (a) a clean Si(111) substrate, and for (b) an 8-TL CaF_2 film deposited at 750 °C. The inset illustrates the 180° rotation of the Ca and F [110] forward-scattering axes relative to the substrate Si axes.

The resulting modulations in Figs. 1 and 2 are quite strong ($\sim$100%), as predicted by theory. We have assigned all the features as either forward-scattering peaks or higher-order diffraction peaks through either theoretical modeling[19] or comparison to emission at different kinetic energies (e.g., Ca *LMM* at 280 eV). Labeled in Fig. 2 are the signature $(11\bar{1})$, (110), (111), (112), and (001) interatomic axes at $-70°$, $-35°$, 0°, $+20°$, and $+55°$ common to the $(1\bar{1}0)$ planes of both diamond and fluorite structures. Differences between Ca 2*p* and F 1*s* XPD profiles result from the different electron kinetic energies (905 and 565 eV), different electron-scattering strengths of Ca and F atoms, and different atomic arrangements near each emitting atom. While Ca has a unique bulk site within a (111) F-Ca-F triple layer, F has two distinct emitter sites, in the upper and lower planes of each triple layer. Hence, the measured bulk F emission is an incoherent average of two separate diffraction profiles. The asymmetry in the F 1*s* profile at $\theta=0°$ is attributed to the polarization asymmetry inherent in the experimental placement of the x-ray source.

Silicon has two distinct bulk emitter sites due to the (111) double-layer structure. Si 2*p* emission from a clean substrate, dominated by bulk atomic sites due to the large escape depth of $\sim$23 Å, exhibits strong forward focusing peaks that are a mirror reflection of CaF_2's. The clearly identifiable peaks in Fig. 2 at polar angles of opposite sign confirm the well-known type-*B* overlayer growth of CaF_2 on Si(111),[20] in which the crystallographic axes of the overlayer are rotated 180° about the [111] direction relative to the Si substrate. The interfacial origin of this overlayer rotation is discussed in Sec. III.

For thick and monolayer films, which exhibit a single component in core-level spectra, the XPD amplitude was obtained as a function of emission angle by subtracting the inelastic background intensity at a higher kinetic energy from the photoemission intensity at the core-level peak. For intermediate thicknesses of CaF_2, the Ca 2*p* core-level spectrum exhibits a well-resolved interface binding-energy shift of $\sim$3 eV (Refs. 10 and 12) (see Fig. 4). To discriminate interface from bulk and surface XPD modulations, a complete core-level spectrum was collected at each polar angle, and component intensities were obtained by automated curve fitting to binding energies determined from high-energy-resolution spectra. Empirical bulk and interface line shapes were derived from spectra taken on thick ($\sim$700 Å) and monolayer films. Analytic Voigt line shapes could not be used for component analysis due to satellite structure in the interface spectra (Sec. III).[13]

C. Structural characterization

In this study, XPD characterization of thin-film morphology relies primarily on the appearance and amplitude of the forward-scattering (FS) peaks, which dominate the photoelectron angular structure at electron kinetic energies greater than few 100 eV.[6–8] This study concentrates on information obtained from Ca 2*p* XPD, although consistent results were also obtained from

fluorine emission (Sec. V). The Ca 2p results are simplest to interpret due to the single Ca emitter site in each layer and the large energy splitting between the bulk and interface components. Multiple emitter sites and the bulk sensitivity of the substrate signal limit quantitative structural information from F or Si XPD. Cluster-scattering calculations including a spherical-wave corrections and double scattering[19] were performed to aid in data interpretation.

Figure 3 illustrates the separate theoretical Ca XPD contributions arising from the surface and two subsurface (111) CaF_2 layers. Surface Ca atoms are uncovered and hence exhibit a flat, unmodulated XPD profile apart from $[\bar{1}\bar{1}3]$ and $[11\bar{1}]$ intralayer Ca→F scattering peaks at grazing angles. For emission from Ca atoms buried by a single overlayer, [100], [111], and [110] FS signatures appear. Emitters buried by *two* or more overlayers in the fluorite structure exhibit an additional Ca→Ca [112] FS signature at $\theta = -20°$ that is absent for the singly buried layer. Deeper buried layers look essentially the same as Fig. 3(c) except for effects of multiple scattering and of enhanced inelastic attenuation at grazing angles. In Fig. 3(c) double scattering along the [110] chain of Ca atoms results in a narrower width and a reduced amplitude of the FS peak compared to the first subsurface layer. Uncovered layers have a flat attenuation profile, while deeply buried layers exhibit $\exp(-z/\lambda\cos\theta)$ attenuation [see Eq. (1)]. Hence multiple scattering and inelastic attenuation provide complementary information about the morphology of these thin films.

For thicknesses of ~2–5 TL's, the measured bulk and interface Ca XPD profiles are linear combinations of Figs. 3(a)–3(c), depending on film morphology. The amplitude of the central [100], [111], and [110] overlayer FS peaks is inversely related to the amount of unmodulated surface signal present, either from the top of a bulk island or from unburied regions of the interface layer between islands. For example, two layers contributing to the bulk signal will result in an average of the two profiles in Figs. 3(a) and 3(b), reducing the amplitude of the central FS peaks by $\sim\frac{1}{2}$. Similarly, if only half of the interface layer is covered by bulk layers, then the interface emission FS amplitudes will also be reduced by $\sim\frac{1}{2}$. This relationship between FS amplitudes and thin-film morphology is quantified below.

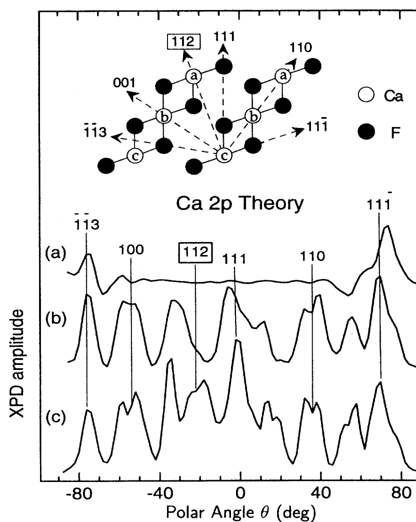

FIG. 3. Theoretical Ca 2p XPD polar profiles for Ca atoms in (a) the surface layer, (b) the first subsurface layer, and (c) the second buried layer. The [112] forward-scattering peak is a signature for the presence of at least two overlayers.

In Sec. IV, we demonstrate a range of initial CaF_2 growth behavior from completely flat films to Stranski-Krastanov (SK) morphologies in which bulklike islands cover a chemically reacted interface layer. In this thin-film regime of <8 ML, substrate attenuation of the Ca 2p bulk-to-interface intensity ratio alone are not sufficient for quantitative characterization of these SK morphologies. Instead, we use a combination of the XPS and XPD measurements, together with the known CaF_2 electron escape depths, to solve for the two quantities of average island height n and fractional island coverage f. The island height n refers to the number of bulk CaF_2 layers above the reacted layer.

In our model, a complete uncovered layer is assumed to contribute unit intensity independent of polar angle (in the approximate range of $-60° < \theta < 60°$), while a layer buried by n overlayers contributes an intensity of $\delta^n[1+\beta(\theta)]$, where δ is the single-layer attenuation factor and $\beta(\theta)$ is the angle-dependent FS enhancement structure. Using XPS, we measure the ratio of the bulk (+ surface) to interface Ca 2p emission from high-resolution spectra taken at the off-axis direction in Fig. 1, which gives values consistent with the ratio of XPD normalization values of the two components. This measured quantity is related to the islanding parameters n and f by

$$\frac{A_{B+S}}{A_I} = \frac{f(1-\delta^n)/(1-\delta)}{1-f+f\delta^n} . \quad (2)$$

Similarly, we can derive an expression for the relative forward-scattering modulation amplitude for bulk (+ surface) and interface signals:

$$\frac{M_{B+S}}{M_I} = \left[\frac{\delta-\delta^n}{1-\delta^n}\right] \Big/ \left[\frac{f\delta^n}{1-f+f\delta^n}\right] . \quad (3)$$

After measuring the two ratios in (1) and (2), we can solve for the two parameters (n,f) on the right-hand sides. The values of n and f are additionally checked for consistency with the expected total deposition, N:

$$N = 1 + nf \quad (4)$$

obtained from the deposition time and calibrated flux. The limitation of this procedure for determining n and f is encountered when the interface intensity becomes too small relative to the bulk peak ($N \gtrsim 6$ ML) and when significant multiple scattering degrades the modulation amplitude. Correlation of the intensity ratio to the modulation-amplitude ratio in Eqs. (2) and (3) is fairly insensitive to the value of the escape depth (34 Å, $\delta \sim 0.91$) used for 905-eV Ca 2p electrons in CaF_2.[21]

III. MONOLAYER STRUCTURE

Monolayer structure is important to our understanding of nucleation behavior; it also serves as the template for overlayer growth. The type-*B* overlayer orientation observed for thick-film XPD originates from the high-temperature monolayer structure, which has previously been determined by ion scattering.[22,23] In this section, we characterize the differing interface nucleation behaviors at high and low substrate temperature, and later in Sec. IV we show that the structure and surface energy of the initial chemisorbed layer governs the nucleation of bulk islands.

A. High temperature

Figure 4 compares Ca $2p$ photoelectron spectra for 0.8-TL and 2–3-TL depositions of CaF_2 at different substrate temperatures. At high temperature [(HT), $>600\,^\circ$C], the Ca $2p$ spectrum in Fig. 4(a) illustrates the well-known $\sim$3-eV interface core-level shift towards lower binding energy.[10,12] This interface component has previously been shown to correspond to Ca bonded to Si at the interface, which also induces a Si $2p$ interface core-level shift to low binding energy.[9–12] The bulk-interface Ca $2p$ splitting is consistently $\sim$2.8–3.0 eV for depositions $>600\,^\circ$C.[24] The intensity of the low binding energy, interface spin-orbit doublet increases at submonolayer coverages and saturates at $\sim$1-layer deposition; this is followed by an increase of the higher binding-energy bulk (+ surface) component. This behavior demonstrates that the chemisorption of the first layer is essentially complete before the onset of bulk nucleation.

While thick film, bulk-sensitive Ca $2p$ spectra are described well by a single spin-orbit Voigt doublet, the $j=\frac{1}{2}$ spin-orbit peak in the submonolayer Ca $2p$ spectra of Fig. 4(b) appears too large and asymmetrically broadened to higher binding energy. A spin-orbit deconvolution of the spectrum (solid line) indicates the presence of an additional component at $\sim$4.5 eV to higher binding with $\sim$25% the intensity of the main peak. The origin of this Ca $2p$ satellite is believed to arise from electronic excitations or F-Ca charge-transfer satellites. These may be excitations across the two-dimensional (2D) interface band gap[25] in the presence of the $2p$ core hole.[26] Regardless of the overall line shape of the monolayer Ca $2p$ spectrum, it is normalized to unit amplitude and used as an empirical line shape for fitting interface Ca peaks in intermediate thickness films. Similarly, a thick-film spectrum is also normalized and used as a bulk line shape. The success at which these line shapes fit intermediate thickness films [see Fig. 4(a)] confirms the continued existence of the monolayer satellite structure upon being covered with bulk CaF_2.

Single-component F $1s$ and Ca $2p$ XPD in Fig. 5(a) confirm the high-temperature chemisorption structure to be a partially dissociated, type-*B* oriented Ca-F layer, resulting from Ca-Si interface bonding. The dashed profiles in Fig. 5(a) show theoretical XPD contributions for each F and Ca emitter site in an isolated (111) Ca-F layer (see inset). The Ca$\rightarrow$F$[\bar{1}\bar{1}3]$ and $[11\bar{1}]$ intralayer scattering identified previously in Fig. 2 is observed in the data for Ca $2p$ emission, Fig. 5(a), clearly indicating that the type-*B* orientation exists at the first layer. The absence of [001], [111], and [110] peaks in the Ca XPD indicates that a second layer has not begun to form. The top, uncovered F site is predicted to exhibit only diffraction minima at $\pm80°$, which come from in-plane F$\rightarrow$F scattering. These dips are also seen in the F $1s$ experimental

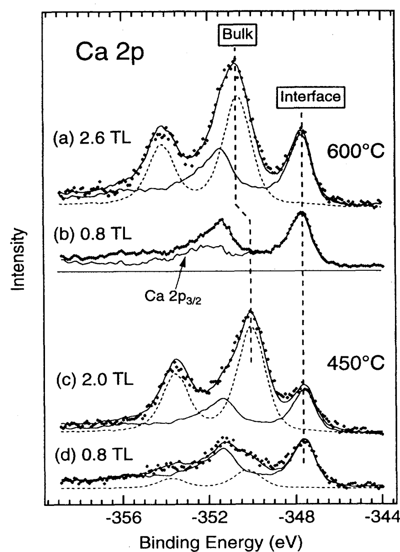

FIG. 4. Ca $2p$ core-level spectra for submonolayer and 2–3-TL CaF_2 films deposited at (a) and (b) high temperature and (c) and (d) low temperature. The dashed profiles in (a), (c), and (d) represent bulk and monolayer line shapes used for component analysis. The Ca $2p_{3/2}$ deconvolved spectrum in (b) illustrates the presence of a satellite excitation at higher binding energy.

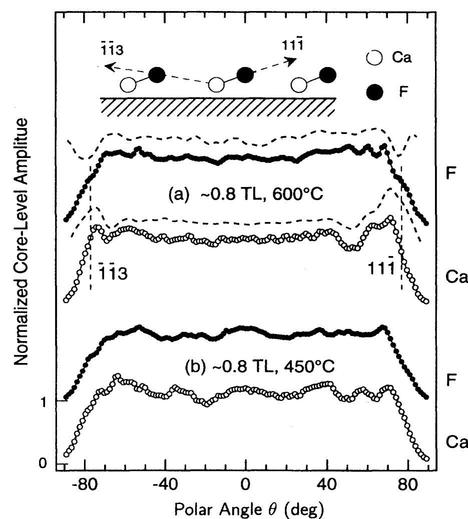

FIG. 5. Submonolayer Ca $2p$ and F $1s$ XPD polar profiles for $\sim$0.8-TL depositions of CaF_2 at (a) $600\,^\circ$C and (b) $450\,^\circ$C. Theoretical Ca and F contributions (dashed) for an ideal Ca-F layer (inset) are also plotted in (a). Vertical lines indicate the onset of geometrical cutoffs of the data.

XPD profile before the onset of a geometrical cutoff of the data at grazing emission (vertical dashed lines). Emission from F atoms in the lower half of a F-Ca-F triple layer would exhibit strong F→Ca and F→F scattering peaks at +70° and −54°. These peaks are distinctly absent in the experimental F XPD profile indicating that, consistent with direct Ca-Si bonding, no ordered F site exists below the interface Ca atoms. Additionally, comparison of the F 1*s*/Ca 2*p* XPS absolute intensity ratio to that for thick-film growth (corrected for inelastic attenuation) confirms a F deficiency and an ~1:1 F:Ca stoichiometry of the high-temperature submonolayer film.

The type-*B* orientation of the chemisorbed Ca-F layer is the template that enforces type-*B* orientation in thick-film growth. The orientation in the chemisorbed layer is most likely enforced by the Si-Ca bonding site and the subsequent low-energy site for the attached F ion. While Ca bonding at T_4 (Refs. 21 and 27) and H_3 (Ref. 27) high-symmetry substrate sites have been observed, forward scattering from the overlayer peaks in this study is not sensitive to lateral registry or interface bonding sites. Type-*B* epitaxy and a T_4 Si-Ca bonding site results in F above an H_3 (hollow) site above the Si interface and the first layer Si near the position of the next F ion in the CaF_2 lattice; type-*B* epitaxy and an H_3 site, on the other hand, places F directly atop a Si atom, which is likely to have higher energy. A uniform type-*B* orientation thus supports the ion-scattering observation of a single T_4 adsorption site.

B. Low temperature

Deposition at substrate temperatures below ~550 °C yields a different monolayer structure, as revealed by XPS and XPD: (i) the Ca:F stoichiometry is approximately bulklike, (ii) the monolayer is not well ordered, (iii) second-layer nucleation of bulk atoms occurs at submonolayer coverages, and (iv) the interface Ca 2*p* component saturates at $\sim\frac{2}{3}$ the intensity of the high-temperature growth. In Fig. 5(b), XPD modulation structure is seen for both F and Ca for 0.8-ML deposition at 450 °C; this structure originates from nucleation of second-layer CaF_2, as confirmed by the onset of a bulk component (~33% of the total intensity) in the corresponding Ca 2*p* XPS spectrum in Fig. 4(d). At 0.5-ML deposition, a small bulk component is also present (<20%), but no coherent FS modulations of F or Ca are seen, thus indicating that Ca→F axes are randomly oriented. Also, we observe faint 7×7 LEED for submonolayer coverages deposited at 450 °C, indicating clustering of adsorbed CaF_2 molecules. In contrast, the substrate reconstruction is removed for ~0.5–0.9-ML depositions at high temperature and 3×1 or 4×1 ordered LEED patterns are observed.

Comparison of the moments of F 1*s* and Ca 2*p* for the high- and low-temperature 0.8-ML depositions in Figs. 4(b) and 4(d) indicates $\sim\frac{1}{3}$ less interface Ca intensity and $\sim\frac{1}{3}$ more interface F intensity at low temperature. For depositions greater than 1 ML, the low-temperature interface Ca component [Fig. 4(c)] saturates at $\sim\frac{2}{3}$ of the high-temperature interface intensity [Fig. 4(a)], indicating incomplete formation of a full monolayer of Ca-Si bonds. The bulk-interface splitting is reduced to ~2.2 eV for low-temperature depositions, but is found to be metastable; with time and exposure to x rays or impurity (oxygen) adsorption, the splitting increases to the larger, high-temperature value. Figures 4(a) and 4(c) show that it is the bulk Ca 2*p* component that shifts with respect to a constant interface binding energy. Similar behavior has been seen in the Ca 3*p* shallow core level for a 500 °C deposition where the larger high-temperature splitting was restored with electron-beam exposure.[12] The high-temperature monolayer XPD profile and stoichiometry could also be obtained by deposition of 2 ML at 450 °C followed by ~800 °C annealing and desorption of ~1 ML (as judged by the disappearance of the bulk Ca 2*p* component).

Si 2*p* spectra were also taken before and after deposition. Despite being bulk sensitive, a slight rise in the Si 2*p* high-binding-energy tail, indicative of Si-F bonding, was observable after low-temperature deposition, but not after high-temperature deposition. Also, the Fermi-level position relative to the clean Si(111)7×7 surface (monitored with Si 2*p*) shifts by 0.4 eV toward the Si valence-band maximum for high-temperature growth, and by only ~0.3 eV for growth at 450 °C.

From comparison of the monolayer results, we postulate the following model. At low temperature, chemisorption (formation of Ca-Si bonds) still occurs but F dissociation either does not occur or leads to F adsorption on the Si substrate. The additional F atoms (and/or Si-F bonds) create a defective submonolayer that blocks $\sim\frac{1}{3}$ of the available Si-Ca bonding sites and inhibits surface diffusion, resulting in early second-layer bulk nucleation. The incomplete interface Ca occupation changes the dipole at the interface, affecting the Fermi-level position and the Ca bulk-interface splitting. Second-layer bulk nucleation begins to order the underlying interface and the additional $\sim\frac{1}{3}$ TL of fluorine gets trapped near the substrate. At high temperature, in contrast, dissociative removal of one F atom per molecule and the formation of a well-ordered Si-Ca-F interface layer is completed prior to any second-layer nucleation. An alternate source of defects in the low-temperature regime, imaged recently by scanning tunnel microscopy (STM),[28] is the four excess Si atoms per 7×7 unit cell. If each of these Si-induced defects blocks three Ca-Si bonding sites, then an $\sim\frac{12}{49}$ or ~25% decrease in the saturation coverage of the first layer would be observed. Bonding of F to these Si defects would also explain the slight high-binding-energy tail in Si 2*p* spectra.

IV. THIN-FILM MORPHOLOGY

A. Component-resolved XPD

The key parameters that determine the initial morphology of CaF_2 growth on the reacted interface layer are temperature and flux. Having established the bulk and monolayer structure of CaF_2 on Si(111) with single-component XPD, we next characterize intermediate

thickness morphologies for different growth conditions using bulk- and interface-resolved XPD and the quantitative analysis outlined in Sec. II C. Figure 6 shows component-resolved Ca 2*p* XPD results for a sequence of growths at (a) high temperature, low flux (HT/LF), (b) high temperature, high flux (HT/HF), and (c) low-temperature (LT) growth conditions. For the data in Fig. 6, HT means $T \approx 700\,^{\circ}\mathrm{C}$, LT means $T \approx 450\,^{\circ}\mathrm{C}$, HF means flux ≈ 50 Å/min, and LF means flux ≈ 5 Å/min; the generic notation refers to broader regions of temperature and flux exhibiting similar growth morphologies, as discussed in Sec. VI.

The HT/LF films [Fig. 6(a)] display strikingly weak diffraction modulation of the interface emission relative to that of the bulk. This suggests the existence of large uncovered regions of a single monolayer. Patches of interface disorder are unlikely due to the strong (ordered) overlayer XPD modulations. With greater deposition, the island thickness ($\sim$bulk XPD amplitude) increases faster than the island coverage ($\sim$interface XPD amplitude), leading ultimately to severely islanded films. Results of the quantitative analysis of the island thickness and interface coverage parameters n and f for each deposition are plotted in Fig. 7 to highlight the relative rates of vertical versus horizontal growth. At 5 Å/min, we see a rapid increase in the average island thickness compared to horizontal coverage. For example, the uppermost growth in Fig. 6(a) represents an average island thickness of ~ 7 TL's covering $\sim 50\%$ of the interface layer, consistent with an overall deposition of 4.5 TL's. Conditions for homoepitaxy ($f=1$) are not expected until well over 10 TL's, at which point the morphology will be very rough.

The islanding may be determined not only from the quantitative analysis, but also from the presence of the bulk atoms' [112] forward-scattering peaks in the 3-TL sample. The existence of this peak indicates that the 2 ML of total bulk deposition is distributed as islands at least three-layers high. Also, the greater inelastic attenuation near grazing emission in the bulk profiles compared to the flat profiles of the interface is consistent with three-dimensional bulk islands and a largely uncovered interface layer.

Upon raising the incident flux rate by an order of magnitude from 5 to 50 Å/min, distinctly different behavior of the bulk and interface XPD modulations is observed. The HT/HF films [Fig. 6(b)] exhibit strong forward-scattering modulations of the interface signal indicating complete or nearly complete coverage by overlayers. At 3 TL's, the existence of the [112] peak in the interface but *not* the bulk signal indicates that the bulk islands are exactly 2 layers in height. At 4 TL's the [112] peak appears in the bulk signal with $\sim\frac{1}{3}$ the amplitude of the interface [112] peak as expected for layer-by-layer growth.

The layer-by-layer growth does not begin immediately, however. At ~ 2 TL's the bulk signal has a nearly identical normalized forward-scattering amplitude as for the 3-TL film; the interface modulation is smaller than for the 3-TL film, but still clearly exhibits the [112] peak. Contrary to a flat two-layer film, the data indicate that 2-TL bulk islands cover only part ($\sim 60\%$) of the interface layer. Hence, the deposition sequence in Fig. 6(b) shows the development of flat films proceeding through the formation of 2-TL-thick islands, which coalesce before the beginning of true layer-by-layer growth. The results of the quantitative analysis outlined in Sec. II C,

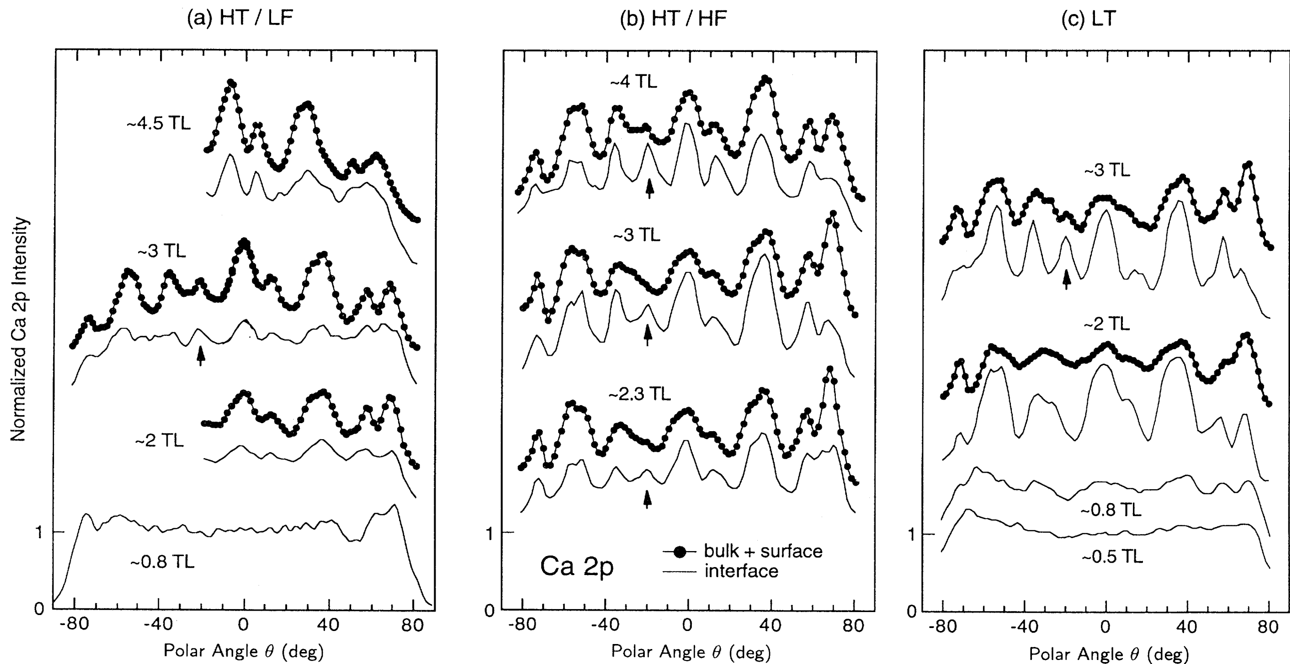

FIG. 6. Bulk- and interface-resolved Ca 2*p* XPD polar profiles for increasing depositions of CaF_2 on Si(111) in three different growth regimes: (a) high temperature/low flux, (b) high temperature/high flux, and (c) low temperature. Vertical arrows indicate the [112] axis. See text for definitions of growth regimes and XPD interpretations.

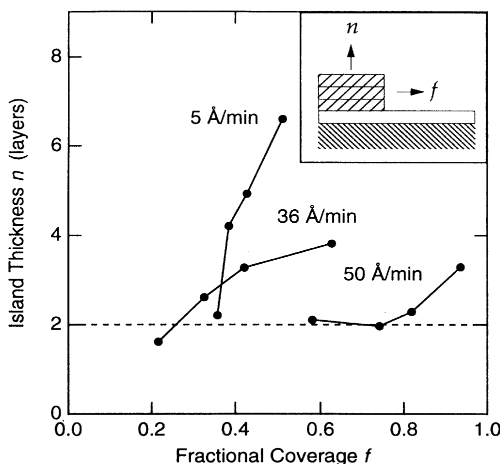

FIG. 7. Quantitative islanding behavior for CaF_2 growth atop the high-temperature interface for three different flux rates of 5, 36, and 50 Å/min. See text for the procedure of obtaining the average bulk island thickness (n) and the fractional coverage of the interface layer (f) from component-resolved Ca 2p XPD.

also plotted in Fig. 7, indicates that burial of the interface layer is not fully achieved until $\sim$4 bulk TL's. This suggests that coalescence of 2-TL bulk islands leaves pinholes to the interface layer that slowly fill in (perhaps only by direct impingement) as third and fourth bulk layers are nucleated.

Deposition of two total layers of material at a lower temperature of 650 °C or a higher flux of 110 Å/min than the conditions for Fig. 6(b) also result in $\sim$50% coverage of the complete interface layer by 2-TL bulk islands, establishing a broader range of the two-layer island stabilization. Depositions at 50 Å/min at the higher temperature of 750 °C or lower fluxes of 36 Å/min show a return to the islanded morphology of Fig. 6(a). Figure 7 additionally shows the HT deposition sequence for 36 Å/min (component-resolved XPD not shown). Here we observe the relative rate of vertical-to-horizontal growth to be intermediate between the HT/LF and HT/HF conditions with homoepitaxy projected at $\sim$4–5 bulk layers.

Films grown at lower temperatures [Fig. 6(c)] show yet a different nucleation behavior. For submonolayer films (0.5–0.8 ML), we identify disorder in the interface layer and nucleation of bulk TL's before the reacted Si-Ca-F_x layer is complete, as discussed in Sec. III B. For thicker films, the interface becomes ordered upon burial by overlayers. The very strong forward-scattering amplitude of the interface signal, even larger than the HT/HF films in Fig. 6(b), indicates complete burial of the interface Ca atoms and equally crystalline films compared to the HT depositions. The relatively weak XPD modulations of the bulk Ca signal at 2–3 TL's and the absence of the [112] peak in the interface emission at 2 TL's suggests the growth to be essentially layer-by-layer immediately. The weak [112] peak in the bulk signal for 3 TL most likely originates from the incomplete ($\sim\frac{2}{3}$) occupation of the interface layer (Sec. III B) forcing nucleation of a third bulk layer (with $\sim\frac{1}{3}$ coverage).

Comparison of the 2-TL and 3-TL depositions at LT also highlights the transition from single scattering through a single layer to multiple scattering through two layers. The [100], [111], and [110] forward-scattering peaks at $-55°$, 0, and $+35°$ all exhibit narrower widths in the interface signal due to double scattering along linear chains of atoms,[29] and the [112] peak becomes well developed. The [11$\bar{1}$] axis at $+70°$ contains multiple scattering along F-Ca-F chains for each additional layer and, hence, exhibits more dramatic defocusing reduction in the forward-scattering amplitude.

Finally, we point out a feature of the atomic structure of the films common to all three regimes. The coincident forward-scattering peaks of the bulk and interface Ca emission in Fig. 6 show that F-Ca-F triple layers stack on top of the interface Ca-F bilayer with bulk spacings and angles. The buried interface structure is identical to both the bulk and the unburied interface, both for flat films and for the buried regions in Stranski-Krastanov-like films. This is contrary to a proposal,[30,31] based on *ex situ* transmission electron microscopy and x-ray scattering, that the buried interface has a more complicated, less dense structure with a two-layer thick $\sqrt{3}\times\sqrt{3}$ buried reconstruction. We have observed a $\sqrt{3}\times\sqrt{3}$ reconstruction, but only upon annealing $\sim$monolayer CaF_2 films in the presence of adsorbed oxygen. Furthermore, the interface model of Lucas, Wong, and Loretto[31] is inconsistent with the XPS shifts we have observed, which we have been able to model successfully by taking into account initial- and final-state effects for the geometry shown.[13,32] The different structure they observe may originate from effects of air exposure or capping with amorphous Si, both present in their study.

B. Low-temperature crystallinity

The characteristics of low-temperature nucleation are found to be relatively insensitive to flux. Growths at 450 °C, 50 Å/min and 600 °C, 110 Å/min exhibited similar XPS and XPD to that shown in Fig. 6(c). At even lower substrate temperatures (or very high fluxes) one expects semiamorphous nucleation to occur. This kinetically limited regime has been characterized with x-ray diffraction and ion channeling by other researchers: at incident fluxes of 40 (Ref. 33) and 200 Å/min,[34] the temperature onset of noncrystallinity was determined to be $\sim$300 °C and $\sim$600 °C, respectively. We limited our investigation of this semiamorphous regime to comparison of bulk Ca emission from 8-TL films for various room-temperature (RT) deposition sequences (see Fig. 8).

Figure 8(a) shows XPD modulations for our standard of crystallinity obtained at HT/HF. Deposition at RT and HF in Fig. 8(b) shows a dramatic decline in forward-scattering amplitude, indicating severe loss of crystallinity. In addition, the profile appears symmetric in polar angle, in contrast to the crystalline HT profile. Upon annealing this RT film to 400 °C [Fig. 8(c)], crystallinity improves, but the polar symmetry is preserved. The symmetric profile indicates an $\sim$equal coexistence of two crystalline domains (type A and B) rotated 180° relative to each other. The presence of mixed domains suggests

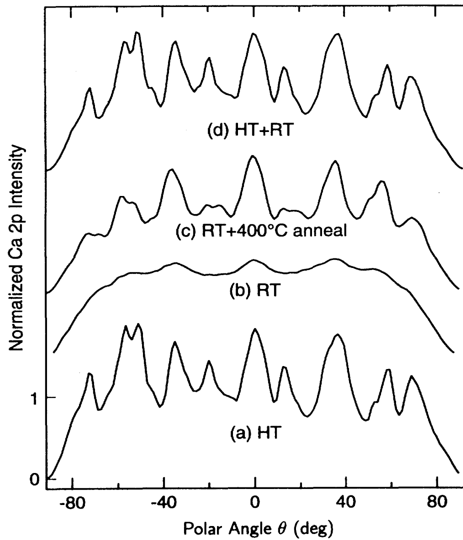

FIG. 8. Bulk Ca $2p$ XPD polar profiles for $\sim$8-TL depositions of CaF_2 films deposited at high flux (50 Å/min) and at (a) high temperature, (b) room temperature followed by annealing (b′), and for (c) a high-temperature template deposition of 4 TL followed by a room-temperature deposition of four additional TL's.

that the starting interface at RT is different (amorphous) than for both the HT and LT depositions, and is likely responsible for the subsequent noncrystalline homoepitaxy beyond 1–2 TL's.

The role of the initial interface structure in controlling room-temperature CaF_2 epitaxy is confirmed by the observation of CaF_2 homoepitaxy at room temperature, previously observed with transmission electron microscopy (TEM) and x-ray diffraction.[4] We confirmed these results *in situ* by investigating a template growth, in which 4 TL's of CaF_2 were first deposited at HT/HF to obtain a well-defined crystalline interface and a bulk-terminated CaF_2 surface. The sample was then allowed to cool to room temperature and an additional 4 TL's were deposited. Figure 8(d) shows identical photoelectron diffraction for this RT homoepitaxy and the HT film. This confirms highly crystalline RT homoepitaxy of CaF_2 once the interface layer is formed, and indicates a high mobility of CaF_2 molecules even at room temperature.

Our observation of mixed-domain type-A and -B growth originating from RT deposition does not explain the observance of pure type-A growth by Cho *et al.*[35] in the temperature range of 100–400 °C or with a ramped temperature-growth condition. We observe that any formation of the chemisorbed Si-Ca-F interface enforces the type-B overlayer domain to the exclusion of type-A domains, which appear to only originate from a loss of crystallinity at the interface.

V. FLUORINE XPS AND XPD

The previous sections concentrated on Ca $2p$ photoemission and bulk- and interface-resolved XPD to establish CaF_2/Si(111) growth morphologies. This is because of (a) the unique structural emitter site of Ca atoms in the bulk crystal, and (b) the large binding-energy-shift signature of interface Ca atoms. Fluorine-atom electron emission is more complicated to interpret due to the existence of two nonequivalent bulk emitter sites and smaller kinetic energy shifts of interface-related species. In Figs. 9 and 10, we present fluorine core-level and Auger spectra and component-resolved XPD for $\sim$3-TL depositions of CaF_2 in each of the three growth regimes of Fig. 6. For completeness, we discuss the effect of interface structure and morphology on fluorine XPS and show the fluorine XPD results to be consistent with Ca $2p$ interpretations.

First we focus on the emission signatures from interface layer F atoms. For F $1s$ spectra [Fig. 9(a)], only at HT/LF can two components be clearly discerned. The low-binding-energy component (LBE) increases at submonolayer coverages and saturates after 1-TL deposition similar to the interface Ca $2p$ LBE component. From our knowledge of the islanded growth morphology in this regime from Ca $2p$ emission, we can surmise that the splitting is most likely related to uncovered F atoms in the interface layer. Indeed if this HT/LF spectrum is component resolved for each polar angle as in Fig. 10, we verify that the LBE component has no forward-scattering peaks, identifying it to be emission from an uncovered layer. Emission from buried interface fluorine is not resolvable, as confirmed by the absence of a clear interface signature in the laminar HT/HF and LT growth regimes.

The absence of a resolvable F $1s$ core-level shift for the laminar regimes precludes the use of F $1s$ component-

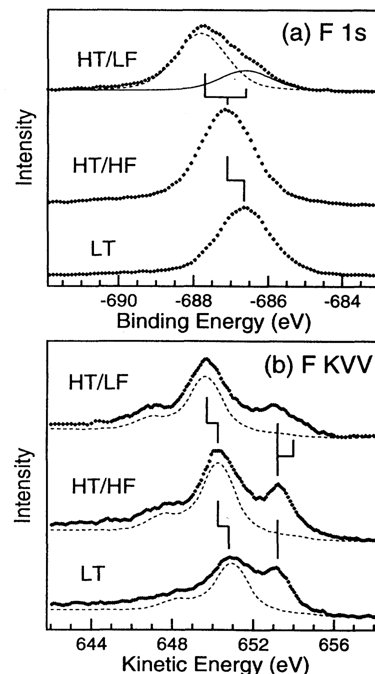

FIG. 9. (a) F $1s$ and (b) F KVV spectra for 2-TL depositions of CaF_2 in each of the three main growth regimes of Fig. 6 illustrating how morphology and interface structure affect peak-energy positions.

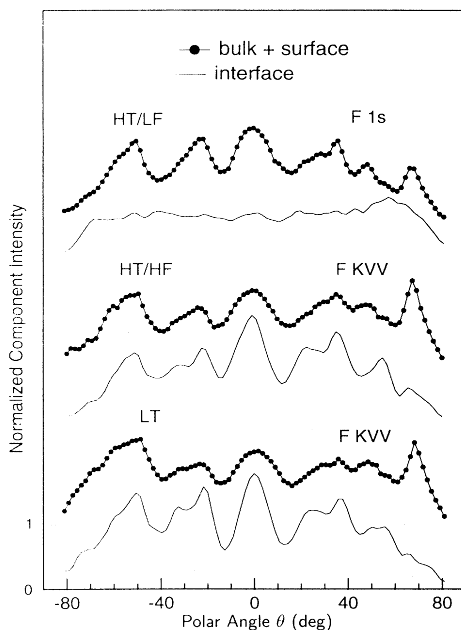

FIG. 10. Bulk- and interface-resolved fluorine XPD for ~3-TL depositions of CaF_2 in the three main growth regimes of Fig. 6. Only in the islanded regime at HT/LF can two F 1s components and two F *KVV* interface components be resolved.

resolved XPD. However, the kinetic energy shift between interface and bulk emission in the fluorine Auger spectra is ~3 times larger than for the 1s spectra; this arises from the additional contribution of final-state relaxation in the presence of *two* final-state core holes in the Auger process, compared to the single-hole photoemission process.[13] Figure 9(b) shows distinct high-kinetic-energy peaks in F *KVV* spectra visibly separated by ~2–3 eV from the main peak in all three growth regimes. The dashed profile in Fig. 9(b) represents a bulk F *KVV* spectrum taken from a thick, 700-Å CaF_2 deposition. Because of the complicated line shape of this bulk Auger spectrum originating from transitions between $L_{2,3}$ and K levels, we quantify and component resolve these spectra using normalized bulk and monolayer line shapes.

The two laminar growth regimes, HT/HF and LT, exhibit very similar component-resolved F *KVV* XPD profiles (see Fig. 10). The large forward-scattering modulations of the high-kinetic-energy peak confirm its origin to be from buried interface F atoms. However at HT/LF, the high-kinetic-energy peak reveals weak but distinct XPD modulation (not shown) in contrast to the absence of XPD structure in the F 1s interface component of Fig. 10. A closer look at the F *KVV* spectrum reveals a third peak ~1 eV to higher kinetic energy from the main interface component. Resolving the HT/LF spectrum into three F *KVV* components as in Fig. 9(b), reveals that the highest energy component (~654 eV) is not modulated; thus we assign its origin to be the unburied interface layer F atoms whose binding energy was resolvable in the F 1s spectra. The intermediate-kinetic-energy component at ~653 eV shows forward-scattering structure and thus corresponds to interface F atoms buried beneath bulk CaF_2 islands.

Additional subtle features exist in the Ca 2*p* spectra of Fig. 4 and in the F 1s and F *KVV* spectra of Fig. 9 and have been quantified by making use of XPD forward scattering to enhance our XPS resolution. In particular, spectra components with different XPD fingerprints are highlighted in the comparison of spectra on and off a known forward-scattering direction of one component. Once the energy position is identified, then component-resolved XPD facilitates positive assignment of the spectral component. The details of this method, which allows spectral components with less than 0.5-eV energy shifts to be distinguished despite a larger source band width (~0.7 eV for Mg $K\alpha$) or larger intrinsic component linewidths, are beyond the scope of this discussion and are published elsewhere.[13] Instead we list the major resolved features: (1) A small ~0.5-eV shift to higher binding energy between unburied and buried Ca atoms has been identified in HT Ca 2*p* spectra. (2) Bulk and interface Ca *LMM* components have been resolved despite large intrinsic peak widths. (3) Surface components of Ca 2*p* and F *KVV* have been separated from the main bulk components and CR-XPD is consistent with the surface assignments. (4) A F *KVV* component intermediate between bulk and interface energies [~651.5 eV in Fig. 9(b)-HT/HF] is shown to exist, and CR-XPD identifies the structural site to be second-layer F atoms residing just above interface Ca atoms. This second interface F site (I_2) further confirms that the buried interface structure is identical to the bulk structure apart from the absence of a F layer below the Ca, as discussed in Sec. IV A. However, the intensity of this I_2 component is consistently ~0.5–0.67 the magnitude of the main I_1 interface component for all HT films. This partial depletion of F atoms adjacent to the interface layer has possible consequences for stability and electrical properties. Interface defects which flatten (pin) the *C-V* curves for high-temperature films may originate from this second F layer. Also, an ordered array of $\frac{1}{3}$ layer of these F vacancies may account for the buried $\sqrt{3}\times\sqrt{3}$ reconstruction observed with TEM.[30]

Finally, we comment on the absolute energy positions of F 1s and F *KVV* spectral components. Similar to the Ca 2*p* bulk and interface components in Fig. 4, the buried I_1 fluorine interface energy is constant between the three different growth regimes, while the bulk (+ surface) component varies. These bulk component shifts are likely related to the change in the interface dipole resulting from the different interface layer stoichiometries between LT, laminar HT, and islanded HT growth regimes. Because the interface peaks do not exhibit overall shifts we cannot attribute the effect to different levels of sample charging.

VI. GROWTH KINETICS DISCUSSION

A. Kinetics phase diagram

Having classified CaF_2/Si(111) growth morphologies for different regimes, we are now in a position to discuss their possible origins in terms of kinetic parameters. Fig-

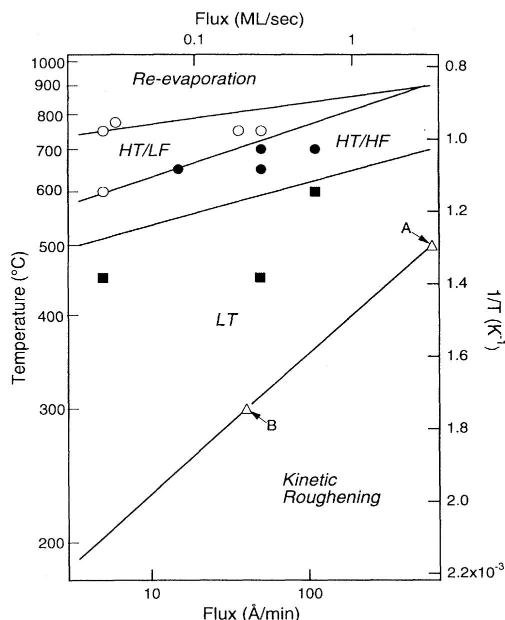

FIG. 11. Schematic dependence of CaF_2/Si(111) growth modes on substrate temperature and incident flux. Arrhenius-like border lines are based on observed growth conditions studied here (points); values taken from the literature (A,B); and from a HT terrace nucleation model required to pass between points C and D.

ure 11 summarizes the dependence of the growth modes on the kinetic parameters of substrate temperature T and incident flux J for isothermal and isoflux growth conditions. This kinetics phase diagram is plotted as $1/T$ versus log J in order to divide the growth regimes with straight lines; this represents an Arrhenius scaling between thermally activated processes, such as diffusion and evaporation, which depend exponentially on $1/T$, and mobile adatom concentration, which is linearly influenced by the incident flux, J. We qualitatively discuss the placement of these broad kinetic transition lines and then apply a nucleation model to our system to understand the division between the HT/LF and HT/HF modes and to derive quantitative parameters. First, we discuss the two extremes of Fig. 11 labeled reevaporation and kinetic roughening.

The uppermost regime in Fig. 11, where no growth occurs, results from reevaporation of incident CaF_2 molecules. The transition border is based on sublimation losses of F and Ca XPS intensity observed upon annealing deposited films for ~1-min intervals at 600, 700, 750, 775, and 800 °C. A deduced sublimation rate of ~1 Å/min at 775 °C was also consistent with two samples grown at 775 °C, in which reevaporation competed with a ~5 Å/min incident flux rate. The actual depositions of 3.1 and 4.4 TL for 2- and 3-min exposure times, as determined by Eq. (4), were smaller by rates of approximately 0.4 TL/min (1.2 Å/min) compared to the predicted coverages of 3.8 and 5.7 TL. Hence, the transition line at which reevaporation begins to compete with the incident flux is drawn to pass through the point (5 Å/min, 775 °C) in Fig. 11 and is scaled to higher temperature at higher flux.

The lower right-hand regime of Fig. 11 represents conditions in which incident species have insufficient energy to overcome barriers or insufficient time to diffuse to their low-energy crystalline sites. The border of this semiamorphous regime is based on previous ion channeling and x-ray diffraction studies determining the two points labeled A (Ref. 34) and B.[33] In our experiments, XPD revealed a loss of crystallinity for room-temperature deposition as well as the presence of mixed domain (types A and B) overlayer orientations, not present in crystalline films deposited at higher temperature. We qualify the description of this *isothermal*-growth regime as the kinetic limitation of the formation of crystalline interface buffer layers for subsequent homoepitaxy, since the *nonisothermal* template growth discussed in Sec. IV B gave evidence for crystalline CaF_2 homoepitaxy at room temperature.

Above this transition line lies the LT growth regime, in which crystalline epitaxy is observed despite the observation of submonolayer disorder, incomplete F dissociation at the interface, and immediate nucleation of bulk layers without the completion of the template interface layer. Second-layer bulk nucleation orders the underlying interface and the additional $\sim\frac{1}{3}$-ML fluorine gets trapped near the substrate in a metastable fashion. The result is an interface whose electrical properties are sensitive to further thermal processing,[36] electron-beam exposure,[12] and also to continued x-ray excitation during XPS analysis (Sec. III B). The overlayer orientation is type B, similar to the high-temperature regimes.

Above ~550–600 °C the reacted Si-Ca-F interface layer forms in an ordered fashion with complete dissociation of the second F atom form incident CaF_2 molecules. Very different bulk nucleation behavior is observed on this layer in the low- and high-incident flux regimes. The upper left portion of the diagram represents an approach to thermodynamic equilibrium, in which species have sufficient energy and time to diffuse to their low-energy sites. Islanding in this HT/LF regime shows that the usual thermodynamic-surface-energy wetting argument is incomplete. The low surface energy of the (111) face of CaF_2 compared to other faces and to Si(111) (Ref. 37) predicts layer-by-layer growth; a simple explanation using the same thermodynamic arguments is that the early formation of the reacted Si-Ca-F layer creates a new surface for subsequent growth whose surface energy must also be taken into account. The reduced Ca charge state[38] in the interface layer leads to a reduced electrostatic binding energy of CaF_2 on Si-Ca-F relative to CaF_2 on CaF_2. Hence, bulk CaF_2 may not wet the Si-Ca-F interface layer and interlayer mass transport away from the interface leads to bulk islanding. A second possible contribution to this growth mode may come from the lattice mismatch present at HT (2.5% at 700 °C) resulting in a favorable reduction in strain energy by the formation of bulk CaF_2 islands.[39] A third possible mechanism for the observed islanding involves the kinetic dependence of the relative nucleation rates atop bulk CaF_2 and atop the Si-Ca-F interface layer. A small decrease in diffusion energy

barriers resulting from the reduced Ca charge can result in a large increase in the single mobile adatom diffusion coefficient, which as discussed further below can affect the nucleation rate.

The influence of kinetics on the HT growth modes is illustrated by the dramatic change to laminar growth at higher flux. At higher flux, the probability of adatom collisions is increased, and appears sufficient to nucleate two-dimensional bulk CaF_2 islands atop the Si-Ca-F interface layer terraces. This terrace nucleation forms sinks for migrating molecules and leads to rapid lateral growth and coalescence of the bulk CaF_2 islands, resulting in complete coverage of the interface layer by ~4-TL total deposition. The observance of a minimum film thickness of interface + 2 bulk TL's in the HT/HF regime may be explained by a net flux of CaF_2 molecules jumping up from the interface layer to form a second bulk layer due to the lowered binding energy of CaF_2 to the interface layer as compared to bulk layers.[40] Upon lowering the incident flux, uninhibited diffusion to and incorporation of CaF_2 molecules at step edges may compete with and suppress terrace nucleation. Rather than leading to layer-by-layer step-flow growth, again, the reduced affinity to and nonwetting of the interface layer may slow the lateral advancement of the propagating step edge and result in multilayer nucleation and 3D growth confined to step edges. The reduced binding energy and increased diffusivity of CaF_2 molecules on the Si-Ca-F interface layer would also drive the formation of this chemisorbed layer to near 100% completion before the initial nucleation of the first bulk layer, as observed in both the LF and HF regimes.

This model of step-edge nucleation (3D growth) competing with terrace nucleation (2D growth) is supported by plan-view TEM images of thicker films (~15-TL deposition) in which strain relaxed regions exhibit Moiré fringe contrast.[41] For HT/LF relaxed regions are observed along lines spaced ~1 μm apart, which are interpreted to be the step spacing on these highly oriented silicon wafers. In contrast, for HT/HF, the relaxed regions are uniformly distributed across the sample surface with little or no detectable correlation to the underlying step structure.

B. HT nucleation model

The transition line in Fig. 11 dividing the HT/LF and HT/HF regimes is based on a growth model by Myers-Beaghton and Vvedensky (M-V),[42] constrained by our experimentally observed initial growth morphologies. In the M-V model, lateral interactions of mobile adatoms are incorporated in the form of diatomic island formation. This island formation was shown to dramatically decrease the effective diffusivity of adatoms and to significantly affect the adatom concentration profiles along terraces. While M-V used their model to explain the transition from step propagation to terrace nucleation growth regimes in GaAs(001) homoepitaxy over a wide range of growth temperatures, fluxes, and terrace misorientation angles, we apply it here to quantify the transition from the 3D islanding at step edges to laminar terrace nucleation growth regimes in CaF_2 on Si-Ca-F epitaxy.

In the M-V model, two competing time scales affecting nucleation are τ_D, the diffusion time for an adatom to reach a step, and τ_A, the interarrival time for incident atoms to land on a site. The diffusion time increases quadratically with the terrace width h, and inversely with the diffusion coefficient D, whose temperature dependence follows from a simple hopping model as

$$\tau_D = \frac{h^2}{D} = h^2 \frac{n_0}{\nu} e^{+E_D/k_B T} , \tag{5}$$

where ν is the attempt frequency for hopping, and E_D is the energy barrier for site-site hopping. The interarrival time is dependent on the density of adsorption sites n_0 [$=7.8\times10^{14}$/cm^2 for Si(111)] and is inversely proportional to the incident flux J:

$$\tau_A = \frac{n_0}{J} . \tag{6}$$

M-V define three regimes: (a) For $\tau_D > \tau_A$, adatom interactions dominate the nonlinear diffusion equation leading to a high rate of terrace island nucleation; (b) for $\tau_D < \tau_A$, step-edge nucleation competes with terrace nucleation; and (c) for $\tau_D \ll \tau_A$ adatom interactions are negligible and direct incorporation into step edges occurs. If we use the transition between the first two regimes to represent the boundary between the HT/HF and HT/LF CaF_2 growth conditions, then equating $\tau_D = \tau_A$ allows us to define a critical transition parameter (temperature, flux, or terrace width) as a function of the other two experimental parameters. The critical transition temperature T_c[K] can be expressed as

$$T_c^{-1} = \frac{8.62\times10^{-5}}{E_D} \ln\left[\frac{2.8}{Jh^2}\right] , \tag{7}$$

where E_D is measured in eV, J in Å/min, h in cm, and a phonon frequency of $\nu \approx 10^{13}$ Hz has been used for the hopping attempt rate.

The physical parameters in Eq. (7) are constrained by the experimental data. Using a terrace width of $h \approx 1$ μm obtained from TEM images, the line separating the islanded and laminar growth conditions in Fig. 11 corresponds to a hopping barrier of $E_D^{\text{expt}} = 1.33\pm0.06$ eV. This value of the hopping barrier is reasonable when compared to a theoretical calculation of the surface corrugation potential. This potential depends on the effective charge of the interface Ca layer, which we estimate from the photoemission interface shift to be between 1.75 and 2.0, with the excess charge centered in the Si-Ca bond.[13] If we assume pair interactions[43] based on a Coulomb potential ($q_F = -1$, $q_{Ca} = +2$) and the hard-core repulsion and van der Waals attraction potentials[44] characteristic of the equivalent rare-gas atom interactions (Ne for F^- and Ar for Ca^{2+}), we find the binding energy of a CaF_2 molecule is about 1.6 eV on a (fixed) CaF_2 surface, and about 1.4 eV on one with charge distribution $(Si/F)^{-0.75}$ $Ca^{+1.75}-F^{-1}$. These represent upper limits for diffusion barriers using this potential, but the saddle-

point energies are found to be quite small, and additional attractive dipole interactions[43] have been ignored.

The second transition in the M-V theory, defining the step-flow regime, is quantified as $\tau_D < \tau_A / \beta$ where $\beta \approx n_0 h^2$ is a measure of the misorientation angle. The critical transition relation in Eq. (7) is then modified by $Jh^2 \rightarrow \beta J h^2 = n_0 J h^4$. For highly oriented 1-$\mu$m-width Si(111) terraces, $\beta \approx 10^7$, a near-zero diffusion barrier is obtained if this second relation is applied to the HT/HF to HT/LF transition. Alternately, using $E_D = 1.33$ eV obtained above from the first transition, a second extremely small critical flux, $J_c \sim 10^{-6}$ Å/min, is predicted for temperatures between 600 °C and 775 °C. The M-V theory, thus, suggests that yet another CaF_2 growth regime may exist on the high-temperature interface at even lower fluxes than plotted in Fig. 11. However, the h^4 dependence makes the critical flux of the second transition very sensitive to the miscut of the substrate surface; for example, a $J_c > 1$ Å/min is obtained for misorientation angles $> 0.5°$ ($h < 500$ Å). We have not fully investigated the extremes of low incident flux and/or small terrace widths, but we have found islanded growth at 700 °C, 50 Å/min on a 4°-miscut wafer (~50-Å terrace width, which would be predicted to have no terrace nucleation).

The observed islanded growth in regimes with nucleation at step edges, contrary to the step flow found in homoepitaxy under similar kinetic conditions, demonstrates the unique aspects of heteroepitaxy of dissimilar materials. The islanded nature of the CaF_2/Si(111) films may arise from the intrinsic partial dislocations present at interface steps in this type-*B* epitaxy. These defects appear to inhibit growth across steps in very thin films, as seen in TEM images showing islands confined to individual terraces.[4]

C. Relation to other research

Most studies of CaF_2/Si(111) epitaxy have focused on thick-film properties or on monolayer structure, and have not described these morphological transitions occurring during deposition of the first few layers. The deposition rates in such studies have usually been chosen for the convenience of the experiment: high flux rates for thick-film deposition and low flux rates for submonolayer control. However, some corroboration of the growth regimes in Fig. 11 can be obtained from the other studies. As mentioned in Sec. IV B, the transition to kinetic roughening at lower temperature and higher flux is taken from the literature. Two different STM studies showing the presence[45] and absence[28] of rowlike structures are consistent with our LEED observation of $n \times 1$ patterns for HT submonolayer nucleation and the persistence of 7×7 for LT nucleation. Real-time low-energy electron microscopy has recently shown the influence of growth kinetics in the LT regime (600–660 °C), in which an abrupt transition to second-layer nucleation occurs at or before the completion of the first layer.[46] The fractional coverages observed[4] by TEM and XPS in a series of 30-Å/min depositions at 700 °C are similar to the 36-Å/min data reported in Fig. 7, and the islanded behavior at higher temperature observed by Wong, *et al.*[4] is consistent with the HT/LF regime reported here. The coalescence of 2-layer-high bulk islands at higher flux (HT/HF regime) has not been observed elsewhere; we are unaware of other structural studies in this kinetic and thickness regime.

VII. SUMMARY

We have demonstrated that the initial stages of CaF_2 heteroepitaxial growth on Si(111) exhibits a wide range of growth morphologies. The structure of the first, reacted interface layer is controlled by the initial growth temperature, and determines whether the second layer is amorphous (RT) or crystalline (LT and HT), as well as whether it wets before (LT) or after (HT) the first layer is completed. In addition, the nucleation of the second and subsequent layers at high temperature is controlled by a combination of flux and substrate temperature, with laminar growth after the coalescence of bilayer islands at high flux and islanded growth at low flux. This variety of growth modes is explained within a kinetic model for step and terrace nucleation, combined with the special property of step-associated defects at the CaF_2/Si interface.

We have also demonstrated the power of component-resolved x-ray photoelectron diffraction for *in situ* studies of growth kinetics. The combination of chemical and structural information enabled detailed descriptions of the average growth morphologies, and should be widely applicable to other systems.

ACKNOWLEDGMENTS

This research was supported by the NSF (Grant No. DMR-9196216) and by the Department of Energy (Grant No. DE-AC03-76SF00098). U. Hessinger was partially supported by the University of Washington Graduate School Research Fund.

---

*Present address: MS 2-400, Lawrence Berkeley Laboratory, Berkeley, CA 94720.

[1] R. Kunkel, B. Poelsma, L. K. Verheij, and G. Comsa, Phys. Rev. Lett. **65**, 733 (1990).

[2] J. Sudijono, M. D. Johnson, C. W. Snyder, M. B. Elowitz, and B. G. Orr, Phys. Rev. Lett. **69**, 2811 (1992).

[3] J. D. Denlinger, E. Rotenberg, U. Hessinger, M. Leskovar, and M. A. Olmstead, Appl. Phys. Lett. **62**, 2057 (1993).

[4] G. C. L. Wong, D. Loretto, E. Rotenberg, M. A. Olmstead, and C. A. Lucas, Phys. Rev. B **48**, 5716 (1993).

[5] J. D. Denlinger, E. Rotenberg, U. Hessinger, M. Leskovar, and M. A. Olmstead, in *Common Themes and Mechanisms of Epitaxial Growth*, edited by P. Fuoss, J. Tsao, D. W. Kisker, and A. Zangwill, MRS Symposia Proceedings No. 312 (Materials Research Society, Pittsburgh, 1993), p. 207.

[6] W. F. Egelhoff, Jr., CRC Crit. Rev. Solid State Mater. Sci. **16**, 213 (1990).

[7] S. A. Chambers, Adv. Phys. **40**, 357 (1991).

[8]C. S. Fadley, Surf. Sci. Rep. **19**, 231 (1993).

[9]F. J. Himpsel, F. U. Hillebrancht, G. Hughes, J. L. Jordan, U. O. Karlsson, F. R. McFeely, J. F. Morar, and D. Rieger, Appl. Phys. Lett. **43**, 596 (1986).

[10]D. Rieger, F. J. Himpsel, U. O. Karlsson, F. R. McFeely, J. F. Morar, and J. A. Yarmoff, Phys. Rev. B **34**, 7295 (1986).

[11]M. A. Olmstead, R. I. G. Urhberg, R. D. Bringans, and R. Z. Bachrach, J. Vac. Sci. Technol. B **4**, 1123 (1986).

[12]M. A. Olmstead, R. I. G. Urhberg, R. D. Bringans, and R. Z. Bachrach, Phys. Rev. B **35**, 7526 (1987).

[13]E. Rotenberg, J. D. Denlinger, M. Leskovar, U. Hessinger, and M. A. Olmstead, Phys. Rev. B **50**, 11 052 (1994).

[14]A. Ishizaka and Y. Shiraki, J. Electrochem. Soc. **133**, 666 (1986).

[15]A value of 830 °C for the Si $7\times7\leftrightarrow1\times1$ transition is consistently reported in the literature, e.g., A. Ishizaka, T. Doi, and M. Ichikawa, Appl. Phys. Lett. **58**, 902 (1991).

[16]R. F. C. Farrow, P. W. Sullivan, G. M. Williams, G. R. Jones, and D. G. Cameron, J. Vac. Sci. Technol. **19**, 415 (1981).

[17]L. J. Schowalter, R. W. Fathauer, R. P. Goehner, L. G. Turner, R. W. DeBlois, S. Hashimoto, J.-L. Peng, W. M. Gibson, and J. P. Krusius, J. Appl. Phys. **58**, 302 (1985).

[18]Ch. L. Strecker, W. E. Moddeman, and J. T. Grant, J. Appl. Phys. **52**, 6921 (1981).

[19]J. Mustre de Leon, J. J. Rehr, C. R. Natoli, C. S. Fadley, and J. Osterwalder, Phys. Rev. B **39**, 5632 (1989).

[20]T. Asano, H. Ishiwara, and N. Kaifu, Appl. Phys. Lett. **42**, 517 (1983).

[21]This value is determined from the ratio of the Ca $2p$ intensity from a 700-Å film (unenhanced by forward scattering) to that of a ML film; and is consistent with (a) measured NaF escape depths [F. L. Battye, J. Leisegang, R. C. G. Leckey, and J. G. Jenkin, Phys. Rev. B **13**, 2646 (1976)]; and (b) mean-free paths calculated using the imaginary part of the potential in the scattering code (Ref. 19).

[22]R. M. Tromp and M. C. Reuter, Phys. Rev. Lett. **61**, 1756 (1988).

[23]M. Katayama, B. V. King, E. Nomura, and M. Aono, Vacuum **42**, 321 (1991).

[24]The apparent variation in this splitting with film thickness is explained by the 0.7-eV split between the bulk and surface emission. The peak shifts to lower apparent binding energy as the relative intensity of the bulk peak increases with thickness (see Ref. 13).

[25]T. F. Heinz, F. J. Himpsel, E. Palange, and E. Burstein, Phys. Rev. Lett. **63**, 644 (1989).

[26]Eli Rotenberg, Ph.D. dissertation, University of California, Berkeley, 1993; E. Rotenberg, M. Leskovar, and M. A. Olmstead (unpublished).

[27]J. Zegenhagen and J. R. Patel, Phys. Rev. B **41**, 5315 (1990).

[28]T. Nakagama, M. Katayama, G. Selva, and M. Aono, Phys. Rev. Lett. **72**, 1718 (1994).

[29]M. L. Xu, J. J. Barton, and M. A. von Hove, Phys. Rev. B **39**, 8275 (1989).

[30]C. A. Lucas and D. Loretto, Appl. Phys. Lett. **60**, 27 (1992).

[31]C. A. Lucas, G. C. L. Wong, and D. Loretto, Phys. Rev. Lett. **70**, 1826 (1993).

[32]E. Rotenberg, J. D. Denlinger, M. Leskovar, U. Hessinger, and M. A. Olmstead, J. Vac. Sci. Technol. B **11**, 1444 (1993).

[33]C.-C. Cho, H. Y. Liu, B. E. Gnade, and T. S. Kim, J. Vac. Sci. Technol. A **10**, 769 (1992).

[34]T. Asano, H. Ishiwara, and N. Kaifu, Jpn. J. Appl. Phys. **22**, 1474 (1983).

[35]C.-C. Cho, T. S. Kim, B. E. Gnade, and H. Y. Liu, Appl. Phys. Lett. **60**, 338 (1992).

[36]J. M. Phillips and C. Y. Yashinovitz, J. Vac. Sci. Technol. A **2**, 415 (1984).

[37]J. J. Gilman, J. Appl. Phys. **31**, 2208 (1960).

[38]F. J. Himpsel, U. O. Karlsson, J. F. Morar, D. Rieger, and J. A. Yarmoff, Phys. Rev. Lett. **56**, 1497 (1986).

[39]C. Ratsch and A. Zangwill, Surf. Sci. **293**, 123 (1993).

[40]K. H. Ernst, A. Ludviksson, R. Zhang, J. Yoshihara, and C. T. Campbell, Phys. Rev. B **47**, 13 782 (1993).

[41]U. Hessinger, M. Leskovar, and M. A. Olmstead (unpublished).

[42]A. K. Myers-Beaghton and D. D. Vvedensky, Phys. Rev. B **42**, 5544 (1990).

[43]G. Gigli, J. Chem. Phys. **93**, 5224 (1990).

[44]E. A. Mason, J. Chem. Phys. **23**, 49 (1955).

[45]Ph. Avouris and R. Wolkow, Appl. Phys. Lett. **55**, 1074 (1989).

[46]R. M. Tromp and M. C. Reuter, Phys. Rev. Lett. **73**, 110 (1994).

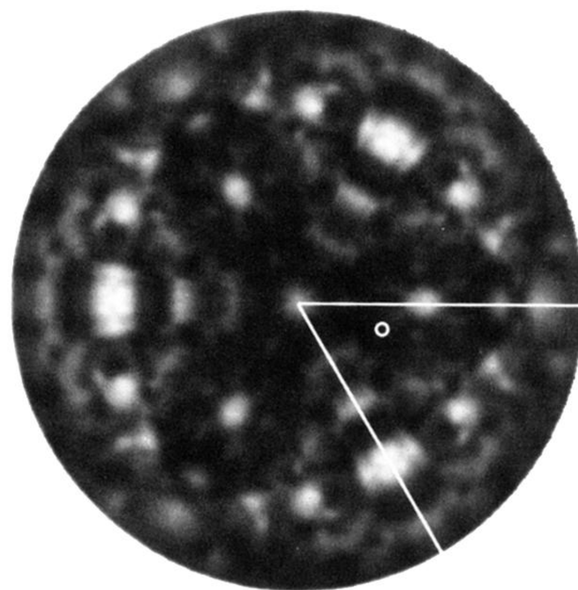

FIG. 1. Ca 2*p* XPD pattern for an 8-TL CaF_2 film on Si(111). Data was collected in the 60° sector shown and then symmetrized to obtain the full 2π planar projection. The white circle indicates an off-axis emission direction used for the intensity analysis without direct forward-scattering enhancements. The CaF_2 film was deposited with a 50-Å/min incident flux at 650 °C substrate temperature.